Steps in gas-surface reactions

Lent, R. van

Chapter 4

Two-faced step edges in HD exchange on Pt

Particle size effects in catalysis are commonly attributed to the number of defect sites present and their electronic properties. Dissociation increases with the number of defects, but how subsequent atomic diffusion at defects influences overall reactivity is generally disregarded. Measuring structure sensitive surface diffusion directly is challenging, especially under reaction conditions, where the kinetics are too fast for most experimental techniques. By using the varying step density of a curved single crystal surface, we instead study how isotopic scrambling of dihydrogen is influenced by step edges. Our results show that step edges lower selectivity towards the HD product compared to terrace sites. We introduce a model that assumes fast isotropic mixing at terraces and no diffusive mixing at steps. The model agrees qualitatively with our data and may provide an additional explanation for lower catalytic activity of very small nanoparticles.

Introduction

Catalysts increase reaction rates of chemical reactions and enable many industrial applications in use today. While heterogeneous catalysts speed up chemical reactions, the reaction mechanisms at play are still not fully understood. Unraveling reaction mechanisms requires systematic study of all elementary steps involved and identifying reaction intermediates. For heterogeneous catalysts, this is exacerbated by the heterogeneous nature of surfaces; elementary reaction steps may be surface-structure dependent.

The simplest heterogeneously catalyzed reaction is isotopic scrambling of dihydrogen. A good catalyst is Pt. The reaction mechanism requires at least three elementary reaction steps: H_2 dissociation, D_2 dissociation, and subsequent recombination to form HD:

$$H_2(g) + 2* \underset{k_{des}}{\overset{k_{ads}}{\rightleftharpoons}} 2H_{ads} \tag{4.1}$$

$$D_2(g) + 2* \underset{k_{des}}{\overset{k_{ads}}{\rightleftharpoons}} 2D_{ads} \tag{4.2}$$

$$H_{ads} + D_{ads} \xrightarrow{k_{des}} HD(g) + 2* \tag{4.3}$$

The heterogeneous nature of the catalyst surface is not captured in these commonly used reaction equations. The stars in the equations indicate surface sites, but do not distinguish between different types. Indeed, previous studies showed that HD formation on Pt surfaces [76–78] is strongly influenced by surface structure. This was explained by increased dissociative sticking of reactants at step edges.

Following several studies [65, 66, 68–70, 75] on the influence of steps, we recently showed that hydrogen dissociation is direct, local, and step type dependent.[79] Reactions 4.1 and 4.2, as the simplest dissociative gas-surface reactions, are thus rather well-understood. However, reaction 4.3 requires that hydrogen (H_{ads}) and deuterium (D_{ads}) atoms be adjacent. Therefore, HD formation is expected to depend on the surface mobility of H_{ads} and D_{ads} and their degree of mixing.

Diffusion on Pt(1 1 1)[80] is fast, as barriers for H_{ads} and D_{ads} diffusion are low: 68 meV and 76 meV respectively[81]. These barriers have been corroborated by theory.[82, 83] Diffusion on Pt(1 1 1) proceeds via two parallel mechanisms: quantum tunneling at low temperature and classical hopping at high temperature.[84, 85] Studies on the influence of surface defects on hydrogen diffusion have been limited[86, 87] due to additional challenges involved.[81, 82] However, theory has predicted that diffusion at steps is anisotropic.[88] Barriers for diffusion parallel and orthogonal to the {0 0 1} step edge are 0.15-0.2 and 0.35 eV respectively, significantly exceeding barriers on the (1 1 1) terraces.[88]

In this study, we resolve whether these larger diffusion barriers influence HD formation on Pt surfaces. Combining molecular beam techniques and a curved single crystal surface approach, we compare locally averaged-step density dependent HD formation and D_2 consumption in a zero (low) coverage limit with initial sticking probabilities. Although both the {0 0 1} (A-type) and {1 1 0} (B-type) steps enhance dissociative adsorption, they are less selective toward enhancing HD formation. Anisotropic diffusion at steps limits diffusive mixing compared to extended (1 1 1) terraces. This is corroborated by increased HD selectivity upon faceting a section of the curved crystal surface. A simple model qualitatively agrees with our results and shows that diffusion of intermediates is integral to the overall reaction mechanism and selectivity toward the HD product.

Method

Experiments are performed in an ultra-high vacuum setup with a base pressure lower than $1{\cdot}10^{-10}$ mbar. The apparatus contains, among others, a quadrupole mass spectrometer (QMS), a supersonic molecular beam with an on-axis quadrupole mass spectrometer for time of flight measurements, and low energy electron diffraction and Auger electron spectroscopy optics. The Pt single crystal surface and the crystal holder are schematically shown in figure 4.1a. The curved surface protrudes from a square holder with two legs attaching it to a liquid nitrogen cryostat. The crystal is cut

as a 31° section of a cylinder with a 15 mm radius, [1 $\bar{1}$ 0] as principal axis, and the (1 1 1) surface at the apex (Z = 0 mm). With the proper cleaning procedure[89], the macroscopic curvature of the surface is a direct consequence of monatomic steps. Consequently, the local surface structure on our crystal varies smoothly from Pt(3 3 5) via Pt(1 1 1) to Pt(5 5 3).[71] As both A- and B-type steps are spatially separated by the (1 1 1) surface, their influence on reactivity can be probed independently.

Reactivity experiments are performed using supersonic molecular beam techniques. H_2 and D_2 are antiseeded in Ar and supersonically expanded from a tungsten nozzle with a 28 µm orifice. The expansion is skimmed. Two additional pumping stages and skimmers produce a rectangular-shaped molecular beam at the sample (6.0 x 0.126 mm^2 or 6.0 x 0.5 mm^2). The H_2 and D_2 mixture is made such that the surface concentrations are equal in the following way. The reaction rate for forming HD, R_{HD}), can be written as:

$$R_{\mathrm{HD}} = k \cdot [\mathrm{H}_{ads}]\,[\mathrm{D}_{ads}] \tag{4.4}$$

where k is the reaction rate constant, and $[H_{ads}]$ and $[D_{ads}]$ are the surface concentrations of hydrogen and deuterium. If we assume low surface coverage, resulting from fast recombinative desorption, and no isotope dependence for adsorption and desorption[18, 66], then the relative surface concentrations are:

$$[\mathrm{H}_{ads}] \propto 2 \cdot \bar{S}_0 \Phi_{\mathrm{H}_2} \tag{4.5}$$

$$[\mathrm{D}_{ads}] \propto 2 \cdot \bar{S}_0 \Phi_{\mathrm{D}_2} \tag{4.6}$$

$\bar{S}_0$ is the local average sticking probability, which depends on step density and by extension on position on the curved surface. It also depends on kinetic energy (E_{kin}). E_{kin} for H_2 and D_2 are approximately 11 and 23 meV respectively, as determined using time of flight measurements. The higher E_{kin} for D_2, decreases its $\bar{S}_0$ by a factor of 1.4.[70] We compensate this by mixing 1.4 times more D_2 into the beam than H_2. Consequently, $[H_{ads}]$ and $[D_{ads}]$ are approximately equal under reaction conditions.

Reactivity measurements are performed with the standard King and Wells approach.[11] The molecular beam forms a 6.0 x 0.126 mm^2 (or 6.0 x 0.50 mm^2) stripe on the single crystal surface. The narrow size of the beam limits the step density convolution along the curved surface. The relative size of the narrow molecular beam and the sample are shown in figure 4.1. Upon being admitted into the main chamber, the beam is blocked by an inert flag. The partial pressures of H_2, D_2, HD, and Ar increase, thereby providing a measure of the background reactivity of the UHV system, e.g. due to hot filaments. After 30 seconds, the inert flag is retracted and the beam directly impinges onto the sample. An increase and decrease in the HD and D_2 partial pressures respectively indicates reactivity toward HD formation by the sample. After measuring HD formation for 30 s, both flags are closed. The sample is subsequently moved 0.5 mm to expose a different section of the curved surface to the molecular beam.

The King and Wells[11] approach works if molecules that scatter off the inert flag and the sample increase the background pressure isotropically. The validity of this assumption requires that the QMS has no line of sight of the beam scattering off either the sample or the inert flag. The curved nature of the surface increases the risk of measuring higher partial pressures due to directional scattering of molecules from the sample into the ionization region of the QMS. The top panel of figure 4.1b shows the evolution of Ar carrier gas throughout the isotopic scrambling experiment. The shaded and hatched sections indicate Ar scattering off the inert flag and the curved crystal respectively. Regardless of whether the beam scatters off the inert flag or the sample, the Ar signal remains constant for each position.

The absolute Ar signal clearly increases over the course of the experiment. The nozzle and expansion pressures are constant throughout the day, ruling out a change in beam conditions. We have previously observed that the absolute QMS signal increases[53] or decreases[90] in a reducing or oxidizing gas for our type of QMS (Baltzers Prisma QMS 200). Comparison of the Ar signal with the HD and D_2 signals in the other panels of figure 4.1

reveal that the relative sensitivity change varies for the different gases. It seems that the change in signal is due to a change in oxidation state of either the QMS filament or the channeltron. The emission current of the QMS filament is regulated, leaving the channeltron as the likely culprit. We suggest that oxidation or reduction of the channeltron material reduces or increases the number of electrons released upon impact. This also explains why the sensitivity change varies seems to be gas-specific, as evidenced by the different relative increases for Ar and D_2 shown in figure 4.1b. During data analysis, we correct for changes in signal by scaling measured data with their background (shaded area) partial pressure.

In addition to Ar, the D_2, H_2, and HD QMS currents are measured for various surface structures by impinging the molecular beam onto different sections along the curved surface. H_2 results are omitted from further discussions as the H_2 background pressures are higher and QMS signals for mass-to-charge ratio of 2 are convolved by D_2. Figure 4.1b compares the raw data of the HD formation experiment for five positions. At every position, we first obtain the background HD partial pressure resulting from all catalytic surfaces, e.g. the nozzle or hot filaments from the sample heating or QMS. Upon impinging the beam onto the surface, H_2 (not shown) and D_2 are consumed to form HD (hatched area).

Results and Discussion

From the raw data in figure 4.1, we extract the relative step density dependent HD formation rate, R_{HD}. We subtract the background production from the total amount and include previous mentioned corrections for the channeltron efficiency. Figure 4.2 shows these HD formation rates at T_s = 500 K and 800 K with our previous $\bar{S}_0$ results (chapter 3) at T_s 155 K and 300 K. HD formation shows the same three characteristics as $\bar{S}_0$: HD rates are lowest for the (1 1 1) surface, increase linearly with step density, and are higher at B-type than A-type step edges. In contrast to $\bar{S}_0$, increasing T_s lowers HD formation slightly. Most striking though, step edges yield an approximate tenfold increase in $\bar{S}_0$ from the apex to the crystal edge, while

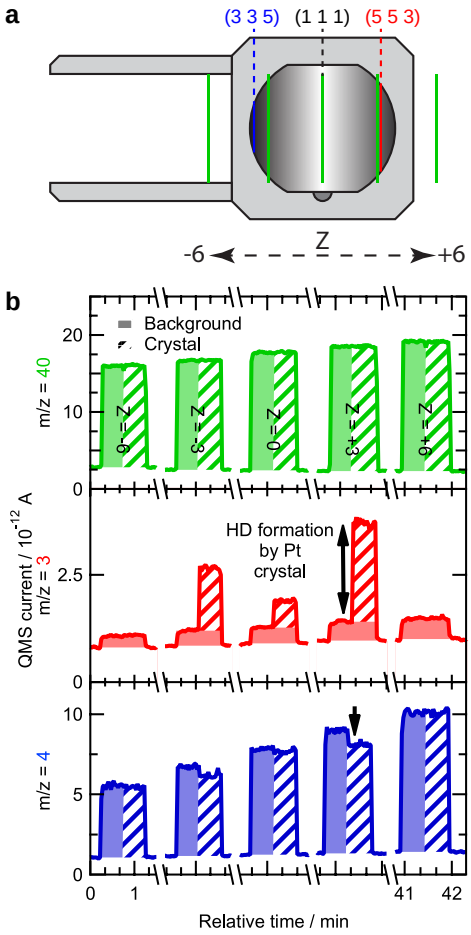

Figure 4.1: King and Wells type HD formation experiments at 800 K. a) The molecular beam (green) impinges onto different parts of the curved surface. The relative sizes of the molecular beam and the sample are to scale. Also indicated are the (3 3 5) (blue) and (5 5 3) (red) surfaces. b) The top, middle, and bottom panels show the raw Ar, HD, and D_2 data respectively for the five different positions indicated in figure 4.1a. The shaded areas show the background signal of HD, Ar, and D_2 after scattering off the inert flag. The hatched areas indicate the beam directly impinging onto the curved sample. The hatched area in the HD signal indicates the HD rate (QMS current) produced by the sample. The fractional drop of the hatched D_2 signal is used to determine $\bar{C}_0$.

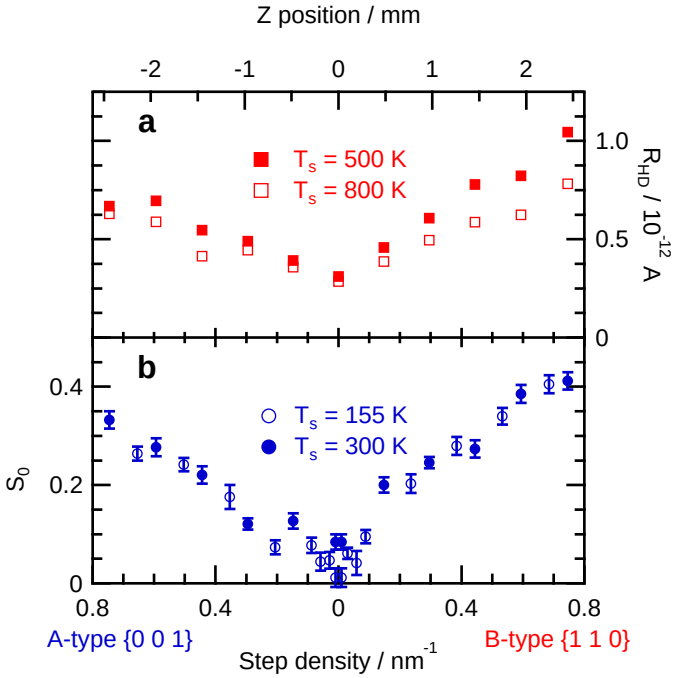

Figure 4.2: a) D_2 initial sticking probability ($\bar{S}_0$) and b) HD rate (QMS current) measured as a function of A- (left) and B-type (right) step density with a 126 μm sized molecular beam.

HD formation only increases roughly threefold over the same step density range for the more reactive step type. Surprisingly, H-D exchange is thus relatively high for the (1 1 1) surface compared to highly stepped surfaces.

A more insightful comparison can be deduced from the drop in D_2 partial pressure in figure 4.1 when HD is being formed (marked by the arrow in the bottom panel). We define $\bar{C}_0$ as the locally-averaged initial consumed D_2 fraction when performing the H-D exchange reaction on the clean surface, akin to initial sticking probabilities ($\bar{S}_0$) as determined by the King and Wells method[11]. Figure 4.3 shows $\bar{C}_0(D_2)$ during HD production as a function of step density for T_s = 500 K and 800 K. Again, $\bar{C}_0$ (D_2) is linear with step density, but increases only a factor of 2-3 over the entire step density range. It varies from 0.04 at the (1 1 1) surface to 0.07 and 0.11 at high A-type and B-type step densities, respectively. Hence, the same

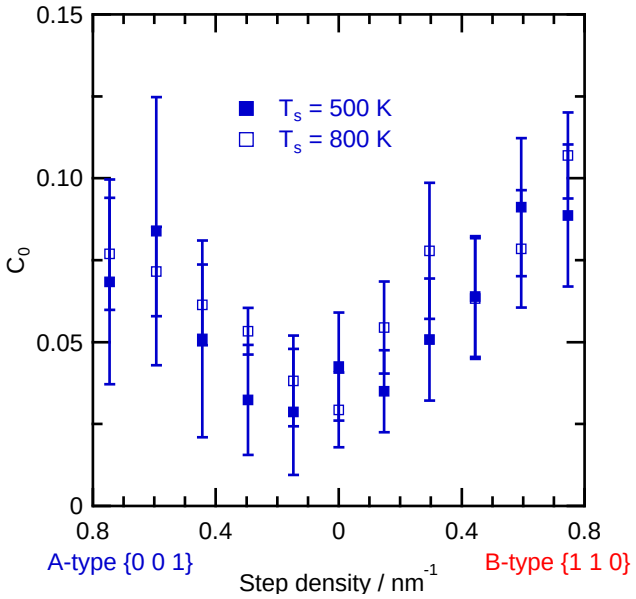

Figure 4.3: D_2 consumption probability ($\bar{C}_0$) during HD production shown in figure 4.2 as a function of step density measured with a 126 μm sized molecular beam.

characteristics observed in HD product formation reappear when analyzing loss of one the two reactants (here D_2). Only the T_s dependence seems lost in the noise.

Variations in how dissociated reactants diffuse may impact the HD rate and $\bar{C}_0$ compared to $\bar{S}_0$ for different reaction sites. We take two extreme cases. For (1 1 1) surfaces we assume fast diffusion leading to isotropic mixing. For steps, we assume no diffusion.

If fast diffusion of equal H_{ads} and D_{ads} surface concentrations leads to an isotropic mixture, the overall surface reaction becomes:

$$2H_2(g) + 2D_2(g) \rightarrow 2HD(g) + H_2(g) + D_2(g) \qquad (4.7)$$

which expresses the statistically expected ratio through the stoichiometric coefficients. From this, it follows that half of the impinging D_2 (H_2) is

consumed to form HD. Hence, the $\bar{C_0}$ (D_2) is:

$$\bar{C_0} = \frac{1}{2} \cdot \bar{S_0} \tag{4.8}$$

Here, we neglect isotope effects. Different zero point energies for H_2, D_2, and HD only slightly alter the H_2, D_2, and HD equilibrium pressures. We justify this choice by realizing that our beam experiments occur on a single collision basis and start with only H_2 and D_2. Since the sticking probabilities are lower than unity (only 0.08 at (1 1 1)), our experiments cannot reach equilibrium.

The situation changes for assumed absence of diffusion at steps. In the limit of no diffusion parallel or orthogonal to the step edge, atoms that originate from the same molecule remain adjacent to one another. Figure 4.4 illustrates how the statistics change. Consider the red step bound atoms as D_{ads} from a dissociated D_2 molecule, while green step bound atoms represent H_{ads} or D_{ads} (originating from either H_2 or D_2). Recombinative desorption of either red atom has a 50% probability to desorb with its original partner, forming D_2. Alternatively, there is a 50% chance that a red atom desorbs with its green neighbor, desorbing as HD or D_2 depending on whether the green atoms were originally an H_2 or D_2 molecule. In the limit of low coverage and no diffusion, absence of green atoms increases the probability of forming back the original molecule. Consequently, 75% of available H and D atoms return as H_2 and D_2. At most, 25% of available H_{ads} and D_{ads} atoms are consumed to form HD in this scenario:

$$C_{0,steps} = \frac{1}{4} \cdot S_0 \tag{4.9}$$

The overall surface reaction at steps becomes:

$$4H_2(g) \; + \; 4D_2(g) \; \rightarrow \; 2HD(g) \; + \; 3H_2(g) \; + \; 3D_2(g) \tag{4.10}$$

The difference between fast and no diffusion thus reveals itself in the fraction η:

$$\bar{C_0} = \eta \cdot \bar{S_0} \tag{4.11}$$

The best case scenarios we have presented here show that fast diffusion and an isotropic distribution of surface bound atoms is revealed by $\eta = 0.5$. Slow anisotropic diffusion at steps may exhibit $\eta = 0.25$ at best. As the ability to mix decreases, so does η.

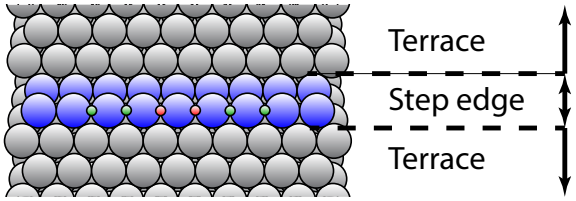

Figure 4.4: Illustration of hindered mixing at steps.

Reactivity measurements at the (1 1 1) surface show $\bar{S}_0 = 0.08$ for $T_s = 300$ K. $\bar{C}_0$ (D_2) = 0.04 indicates that mixing at the (1 1 1) surface is isotropic, $\eta = 0.5$. At high step densities, $\bar{S}_0$ for A-type and B-type step edges shown in figure 4.2 are as high as 0.33 and 0.41. Fast diffusion at steps would result in $\bar{C}_0$ (D_2) equals 0.15 and 0.20. Instead, we find that $\bar{C}_0$ (D_2) equals 0.08 and 0.09, which agrees with limited diffusion at steps. However, large error bars of $\bar{C}_0$ in figure 4.3 prevents reliable η determination. Therefore, we will now present η as a function of step density measured with a larger beam, thereby reducing spatial resolution but improving the signal-to-noise ratio.

To emphasize the influence of local surface structure, we use an extra characteristic of the curved Pt(1 1 1) crystal to our advantage. It contains Pt(9 9 7), which is well-known to exhibit step-doubling and faceting.[89, 91] Both types of reconstructions lower step density and increase the fraction of (1 1 1) terraces. The sensitivity to reconstructions of Pt(9 9 7) requires a specific cleaning procedure for the curved Pt(1 1 1) sample.[53] The correct cleaning procedure yields the desired surface structure with monatomic steps and no faceting. However, reconstructions provide additional means to study the influence of surface structure, e.g. how double high step edges affect reactivity.[92] Here, we anneal the sample to T_s =

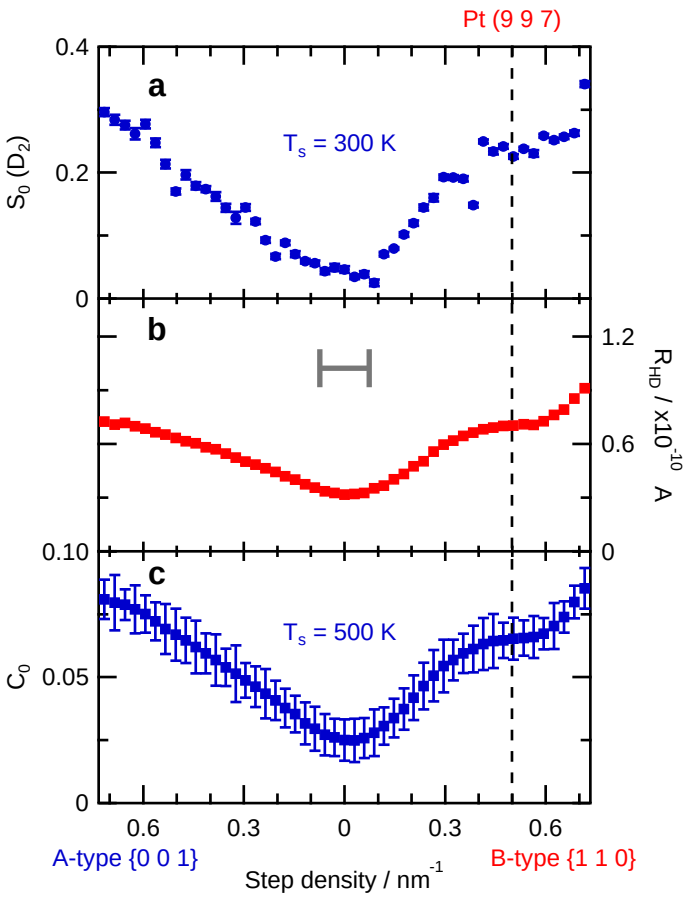

Figure 4.5: D_2 $\bar{S}_0$ at T_s = 300 K. HD formation and $\bar{C}_0$ measured at T_s = 500 K as a function of step density. The crystal is annealed at 1200 K to induce surface faceting near Pt(9 9 7). The gray horizontal error bar illustrates the 500 µm wide beam size convolution.

1200 K and thereby locally facet the sample near (9 9 7)[89], forming extended terraces. Facetting peaks around Pt(4 4 3).[53] The results for $\bar{S}_0$, HD rate, and $\bar{C}_0$ (D_2) are shown in figure 4.5. Here, $\bar{C}_0$ (D_2) are extracted from the D_2 and HD data using the mass balance, as described in appendix C.

Again, at 300 K $\bar{S}_0$ around Pt(1 1 1) is 0.04-0.05 and we measure $3{\cdot}10^{-10}$ A for HD formation. $\bar{C}_0(D_2)$ is 0.025 during HD formation, as

determined from the HD and D_2 signals. $\bar{S_0}$, $\bar{C_0}$, and the HD pressure increase linearly with A-type step density. However, $\bar{S_0}$, $\bar{C_0}$, and HD formation for B-type steps show reactivities that level off around 0.5 nm^{-1} step density, or Pt(9 9 7). The larger beam size convolution makes it difficult to pinpoint over what range faceting occurs, but previous results[53] suggest this occurs at Pt(4 4 3). Using the increased signal-to-noise ratio in these data, we calculate the surface structure dependent HD selectivity, η.

Figure 4.6 shows η results in red, as determined from the results from figure 4.5. η is approximately 2-2.5 times higher for Pt(1 1 1) than highly stepped surfaces. For A-type step edges, the HD selectivity flattens off at approximately 0.30±0.07 nm^{-1} (or 10-17 atom wide terraces). The selectivity for surfaces containing B-type step edges also flattens off, but only does so at 0.6 nm^{-1} (or 6-8 atom wide terraces). While dissociation probabilities are lower for the facetted B-type surface, these surfaces show values for η similar to (1 1 1). Inducing facetting on the B-type side improves selectivity towards H-D exchange.

From the model that describes initial reactant dissociation as a linear combination of steps and terraces[70], we construct a similar model for HD production including the extreme cases of surface diffusion. First, dissociation is described as the sum of dissociation at (1 1 1) terraces and steps:

$$\bar{S_0} = \alpha \cdot S_0^S + (1 - \alpha) \cdot S_0^T \tag{4.12}$$

where α is the relative abundance of step sites. Second, we invoke this same linear dependence for D_2 consumption, but assume the mixing behavior at steps and terraces changes as discussed previously. $\bar{C_0}$ is described as the sum of contributions to HD formation by steps and terraces:

$$\bar{C_0} = \frac{\alpha}{4} \cdot S_0^S + \left(\frac{1 - \alpha}{2}\right) \cdot S_0^T \tag{4.13}$$

where $\frac{1}{2}$ and $\frac{1}{4}$ represent η at terraces and steps. α is determined from the reaction cross sections in chapter 3 for the size of the two types of step

edges. These widths closely resemble the width of the {1 1 3} and {3 3 1} microfacets, as shown in appendix C. We then attribute reactivity at A- and B-type step edges to only the {1 1 3} and {3 3 1} facets. We assume that the sticking probability at steps, S_0^S, is unity as the linear relation of $\bar{S}_0$ with step density predicts (see appendix C). The sticking probability at the (1 1 1) terraces, S_0^T, is 0.0315 as extracted from the same linear dependence. We thus assume:

$$S_0^S = 32 \cdot S_0^T \tag{4.14}$$

This model predicts surface structure averaged values for η:

$$\bar{\eta} = \frac{\bar{C}_0}{\bar{S}_0} = \frac{7.5\alpha + \frac{1}{2}}{31\alpha + 1} \tag{4.15}$$

We convolute the values by averaging over 0.5 mm to simulate the width of the molecular beam.

Figure 4.6 presents the η results from our model in black. We obtain good agreement with experimental results for high A- and B-type step density. The model predicts a slight asymmetry due to the larger reaction cross section for B-type steps than A-type steps. Note that the model does not incorporate the reconstruction centered around Pt(9 9 7) and Pt(4 4 3). Consequently, HD exchange is higher there than predicted by the model. Despite large error bars near (1 1 1), a result of the large relative error in S_0, extended (1 1 1) terraces are significantly more selective towards HD formation than predicted by our simple model.

First, we address why η at the (1 1 1) surface exceeds the highest expected value of 0.5. Our model does not include any T_s dependence for reactivity. It assumes S_0 at 300 K and 500 K are identical. While T_s dependencies reported in literature are generally weak,[18, 66, 68] S_0 increases from 0.12 to 0.14 on Pt(1 1 1) by increasing T_s from 100 K to 300 K[18], albeit at higher E_{kin}. If we assume the same S_0 increase at terraces from $T_s = 300$ K to 500 K, then η lowers by approximately 15% at (1 1 1) and agreement with our model improves.

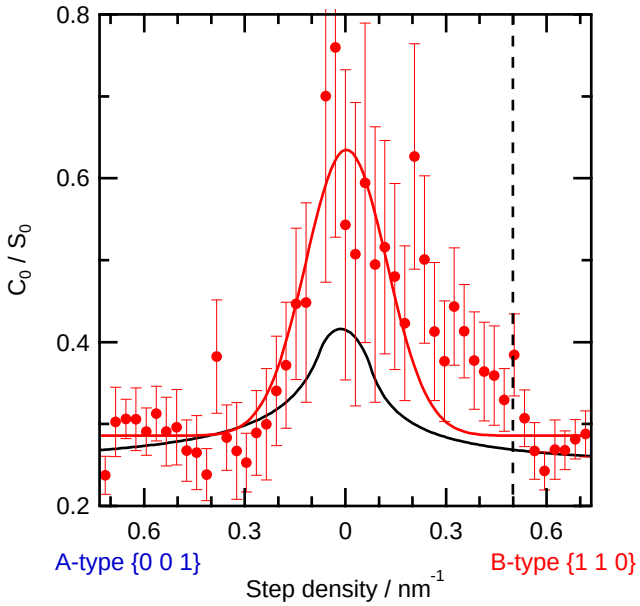

Figure 4.6: HD selectivity as a function of step density. Symbols show the data. The solid red line is a Gaussian fit to the A-type data to guide the eye. The solid black line is calculated from equation 4.15, which assumes different mixing behavior for dissociation at terraces or dissociation at steps.

A T_s dependence at steps manifests itself as a decrease in indirect dissociative adsorption at steps,[66] i.e. the reaction cross section of the step edge will be smaller. We do not observe the significant negative correlation of S_0 with T_s[66] in chapter 3[79] and a T_s dependence for S_0^S cannot explain the overall trend. It would reduce the slope in equation 4.12, but the curvature remains.

Second, η is also significantly higher at intermediate A-type step density than predicted by our simple model. The model assumes isotopic scrambling occurs between identical sites. We explain deviation at lower step density by diffusion between two different sites, i.e. diffusion from steps onto the terrace. As terraces become wider, scrambling is more probable when H_{ads} and D_{ads} can readily diffuse over the (1 1 1) terrace and move farther from the initial reaction site. For narrow terraces, H_{ads} and D_{ads}

may diffuse orthogonal to the step edge but will quickly return to it.

These results highlight the importance of diffusion in catalytic reactions at surfaces. Heterogeneously catalyzed reactions often exhibit particle size dependencies ascribed to the number of (defect) sites available. Diffusion of intermediates is often neglected. As catalyst particles become smaller, reduced catalytic activity is attributed to electronic effects related to coordination numbers.[93, 94] Our results show that limited diffusion of reactants at small terraces also hinders overall reaction kinetics.

Conclusion

In conclusion, we have studied the step density dependence of HD formation using a curved Pt(1 1 1) single crystal surface. By comparing initial sticking probabilities with D_2 consumption during H-D exchange, we show that diffusion is essential in HD formation. By facetting a section of the curved surface, we confirm that extended (1 1 1) terraces improve selectivity toward the HD product. A simple model assuming fast diffusion at terraces and no diffusion at steps is in good agreement with our results. These results show that diffusion is integral to the overall reaction mechanism and may be an additional explanation for particle size effects observed in heterogeneous catalysis.